The 8th Torunian Carbon Symposium, Toruń, Poland, September 2–5, 2009

Domain-Type Collective Dimerization of Graphite and Possible $sp^2 \rightarrow sp^3$ Transition Induced by Inter-Layer Charge Transfer Excitations in the Visible Region

L. Radosinski[a], K. Ostasiewicz[a], T. Luty[a], A. Radosz[b] and K. Nasu[c]

[a]Institute of Theoretical and Physical Chemistry, Wrocław University of Technology
Wybrzeże Wyspiańskiego 27, 50-370 Wrocław, Poland

[b]Institute of Physics, Wrocław University of Technology, Wybrzeże Wyspiańskiego 27, 50-370 Wrocław, Poland

[c]Solid State Theory Division, Institute of Materials Structure Science, High Energy Accelerator Research Organization (KEK), 1-1 Oho, Tsukuba, 305-0801, Japan

We theoretically study possible domain-type collective dimerizations of graphite induced by inter-layer charge transfer excitations in the visible region. Using the semiempirical Brenner theory, we have calculated the adiabatic energy along the path that starts from original two distant graphite layers, but finally reaches the dimerized domain which consists of about 100 carbons with inter-layer σ-bonds. The energy barrier between this new domain and the starting graphite is shown to be of the order of 1 eV, being easily overcome by applying a few visible photons. We have also shown the optimal path of transformation via step by step increase of the domain size.

PACS numbers: 81.30.Hd, 61.66.−f

1. Introduction

Recently, one can observe rapidly growing interest in experimental and theoretical investigations of novel carbon based materials. This is closely related to the peculiar properties of the carbon, developing *sp*, existing in the variety of phases with *sp*, sp^2 and sp^3 hybridization and to the development of new experimental methods involving femtosecond laser pulses that are expected to lead to important applications for medicine, electronics and nanoengineerings [1–3]. Recent experiments [3–5] suggest a possibility of photogeneration of non-equilibrium long-lived (metastable) phase(s) with inter-layer σ bonds between two distorted graphite layers. In Kanazaki's experiment [3, 4], graphite was illuminated by femtosecond pulse of laser light with the energy 1.57 eV polarized perpendicular to its layers. After this illumination, a new buckling domain has appeared: a six member carbon ring was deformed in the way that 4 atoms extruded out of the layer and 2 intruded inside of the layered crystal. The resulting domain, consisting more than 1000 atoms, was stable for several days at room temperature. In the Raman et al. [5] experiment another structural change in the graphite was induced by a femtosecond laser pulse irradiation. Following an initial contraction of the interlayer spacing by less than 6%, the graphite was driven nonthermally into a transient new state with sp^3-like hybridization, involving interlayer bonds. This led to the contraction of the interlayer distance from the initial 3.35 Å (graphite) to final 1.9 Å in a new, photogenerated phase.

These transformations seem to belong to the so-called photoinduced phase transition (PIPT) [6–9]. However, in this case we are uncovering a new aspect of PIPT. Usually, photoexcited electron in an insulating crystal induces a local lattice distortion and such a sudden change of the charge distribution ultimately results in new equilibrium atomic positions within the excited state. This idea is associated with the hidden multistability (Fig. 1): besides its true ground state, a material also possesses a false, metastable one [1, 6]. One can assume that the ground and metastable states are separated by a high energy barrier, which is unaccessible by thermal fluctuations; due to photoexcitation and lattice relaxation, the system may jump from ground state to the metastable one, resulting in new electronic and structural orders. This type of non-equilibrium phase transition has already been observed recently in many organic molecular solids, organic metal-complexes crystals and in the perovskite type compounds [6, 10]. Particular issue of the photogenerated phase transformation observed in [3–5] is the fact that graphite is not an insulating material and PIPT scenario as described above has to be revisited.

In this paper, we will study theoretically a possibility of generation of a novel graphite domain consisting of locally dimerized graphite layers with σ-type inter-layer bonds. We will begin from examining several possible

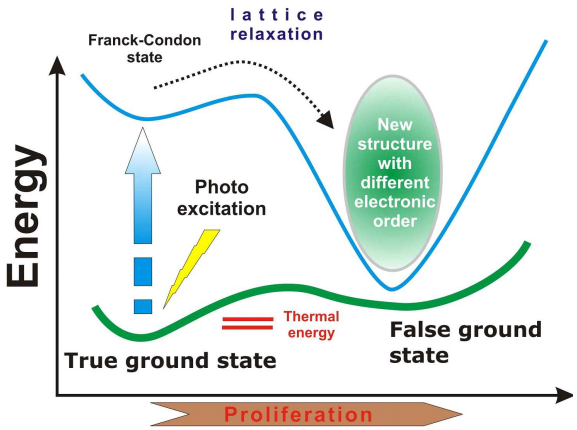

Fig. 1. Schematic idea of photoinduced phase transition. Material besides its true ground state, also possesses a false one, separated by a high energy barrier, which is unaccessible by thermal fluctuations. However due to aforementioned photoexcitation and lattice relaxation, the system may jump from ground state to the metastable one, resulting in completely new electronic and structural orders.

candidates for such a new domain structure and the optimal one will be indicated. Then we will investigate transformation path where initial domain evolves, step by step along potential energy surface.

One can view/consider this phenomenon in a wider context of the graphite–diamond transformation. Theoretical investigations in this area have been undertaken by Cohen et al. [11, 12]. These authors, by means of local density function (LDF) estimated the energy barrier between the graphite and the diamond to be 0.33 eV/atom. This rather large value is due to the $sp^2 \rightarrow sp^3$ inter-layer bond conversion. This fact is manifested in high pressure and high temperature (3000 ℃, 15 kPa) [13, 14] or strong X-ray beams [15] experimental realizations of the direct transformation. In this type of direct synthesis, a large amount of energy is distributed over the crystal, resulting in a global, simultaneous conversion of a macroscopic number of carbon atoms.

Our present problem is different from these global phase transition. We are considering a local and nonequilibrium phase transformation. The main part of the crystal still will persist in its original semimetallic phase, and a newly photogenerated domain with the inter-layer σ-bonds is immersed in it, breaking the translational symmetry of this crystal lattice. The energy barrier to create this new domain is strongly affected by the domain boundary. Unlikely to the case of the conventional global and simultaneous transformation, we will be discussing the case that some translational symmetry of the crystal lattice will be preserved (even at the top state of the energy barrier of the phase transition). The important question of early stage dynamics, involving the problem of localization of excited electron in semimetallic structure will be considered elsewhere.

2. Adiabatic potential energy surface

2.1. Model and method

In our model, we consider two, initially non interacting graphite layers with the ABAB-type stacking. Our new domain, whatever it may be, is immersed in the semimetallic graphite, and hence all the carbons are expected to be always almost neutral. We expect that total number of atoms taking part in this transformation will be about 1000 atoms, and hence the surrounding original graphite has to be at least one order greater than these atoms. To handle such a great number ($\approx$ 10000) of atoms with no translational symmetry, methods like the LDF are no longer realistic, and in fact, prohibitively difficult. Henceforth we employ the semiempirical Brenner potential theory [16]. This potential is widely used in various calculations of carbon and hydrocarbon based clusters. In contrast to the Lennard–Jones two-body type potential theory, the Brenner potential takes 3- and 4-body effects into account as a change of an angle between each bond or as a change of coordination number of each specific atom. The parameter values of this potential are determined semiempirically, so that they take into account almost all existing experimental and theoretical data of carbon clusters [16]. Thus it is appropriate to describe vacancies, interstitials and dislocations in large clusters of neutral carbon atoms.

2.1.1. Brenner's potential

The cohesive energy of material is represented as a sum over the bonds in the following manner:

$$E = \sum_i E_i \,, \tag{1}$$

where E_i is a contribution from atom i. Following Brenner [16], the sum over the bonds used in our research is represented as follows:

$$E_i = \sum_{j(<i)} \left[V_{\mathrm{R}}(r_{ij}) - \bar{B}_{ij} V_{\mathrm{A}}(r_{ij}) \right] . \tag{2}$$

The sum is taken over the bonds between atom j and atom i, with a length ($\equiv r_{ij}$) in between. It consists of the two pair potentials $V_{\mathrm{A}}(r_{ij})$ and $V_{\mathrm{R}}(r_{ij})$ that represent an attractive and a repulsive coupling within the bond, respectively. They are given by

$$V_{\mathrm{A}}(r_{ij}) = \lambda f_{CC}(r_{ij}) D^{\mathrm{e}}_{CC} S_{CC}/(S_{CC}-1) \times \exp\left(-\sqrt{\frac{2}{S_{CC}}} \beta_{CC} \left(r_{ij} - R^{\mathrm{e}}_{CC} \right) \right) , \tag{3}$$

$$V_{\mathrm{R}}(r_{ij}) = \lambda f_{CC}(r_{ij}) D^{\mathrm{e}}_{CC}/(S_{CC}-1) \times \exp\left(-\sqrt{2 S_{CC}} \beta_{CC} \left(r_{ij} - R^{\mathrm{e}}_{CC} \right) \right) , \tag{4}$$

where values of parameters, according to Brenner [16], are given by $R^{\mathrm{e}}_{CC} = 1.315$ Å, $D^{\mathrm{e}}_{CC} = 6.325$ eV, $\beta_{CC} = 1.5$ Å^{-1}, $S_{CC} = 1.29$, $\delta_{CC} = 0.80469$, $R^{(1)}_{CC} = 1.7$ Å, $R^{(2)}_{CC} = 2.0$ Å, $\alpha_0 = 0.011304$, $c_0^2 = 381$, $d_0^2 = 6.25$. They are fitted so they reproduce all known experimental and theoretical data [16]. The parameter λ was fitted

to be $\lambda = 0.49$, so that it reproduces the energy barrier (0.33 eV/atom) obtained by the LDF calculation of Cohen et al. [14], for the ordinary uniform Graphite–diamond transition without changing the bond equilibrium distance. Thus, our theory is consistent with the LDF result, if it is used for the uniform phase transition of an infinite carbon system with the translational symmetry. It is worth to be mentioned that, by setting the parameter at $S_{CC} = 2$, the pair terms reduce to the usual Morse potential with a well depth D^{e}_{CC}. Both the bond coefficient and pair potentials are modulated by the same cut-off function $f_{CC}(r_{ij})$. It simulates the bond formation and the destruction during the transformation, and is given by

$$f_{CC}(r_{ij}) = \begin{cases} 1, & r_{ij} \le R^1_{CC}, \\ \cos^2\left(\frac{\pi(r_{ij}-R^1_{CC})}{2(R^2_{CC}-R^1_{CC})}\right), & R^1_{CC} < r_{ij} < R^2_{CC}, \\ 0, & r_{ij} \ge R^2_{CC}. \end{cases} \quad (5)$$

In the formula above R^1_{CC} indicates the distance where the bond starts to collapse, and R^2_{CC} denotes the final interaction distance.

The crucial part in the Brenner potential, however, is $\overline{B_{ij}}$ factor, which reflects the geometry of the local environment of the bond ij. It is defined by:

$$\overline{B_{ij}} = \frac{B_{ij} + B_{ji}}{2}, \quad (6)$$

where B_{ij} is given as

$$B_{ij} = \left(1 + \sum_{k(\neq i,j)} G_C(\theta_{ijk}) f_{CC}(r_{ik})\right)^{-\delta_{CC}}. \quad (7)$$

As we can see, the value of the coefficient B_{ij} depends not only on a bond length r_{ij} relative to the equilibrium distance ($\equiv R^{e}_{CC}$) but also on the angle θ_{ijk} between the bonds. The angle function $G_C(\theta_{ijk})$ is given by the formula

$$G_C(\theta) = a_0 \left[1 + \frac{c_0^2}{d_0^2} - \frac{c_0^2}{d_0^2 + (1+\cos\theta)^2}\right]. \quad (8)$$

This formula favors both the sp^2 and sp^3 hybridizations where the angles between the bonds are equal to 120° and 109.47°, characteristic to the graphite and the diamond structures, respectively. Although Brenner's potential does not take into account long range (> 2 Å) interactions it does not cause serious mismatch. The transformation occurs only in limited volume (2 layers, 200 atoms each) and the energy difference due to long range interactions is minor. In such case energy contribution due to long range interactions is several orders smaller than due to inter-layer bond formation. Hence in our calculations we focus our attention to predominant process governing the transformation and use of the Brenner potential seems appropriate.

2.1.2. Model

As mentioned above, we consider initially non-interacting two graphite layers (200 × 200 neutral carbon atoms), whose each end is connected by the periodic boundary condition. In Eq. (2), the distance r_{ij} is given by the position vector ($\equiv \bar{\boldsymbol{r}}$) of i-th atom as

$$r_{ij} \equiv |\bar{\boldsymbol{r}}_i - \bar{\boldsymbol{r}}_j|, \quad (9)$$

and $\bar{\boldsymbol{r}}_i$ is defined as a shift from its original position ($\equiv \bar{\boldsymbol{r}}_{i0}$) in the graphite as

$$\bar{\boldsymbol{r}}_i \equiv \bar{\boldsymbol{r}}_{i0} + E_n(\bar{\boldsymbol{r}}_{i0})\left[(\Delta q + \delta B_d(\bar{\boldsymbol{r}}_{i0}))\bar{\boldsymbol{e}}_z + \Delta X \bar{\boldsymbol{e}}_x\right]. \quad (10)$$

The second part denotes the new diplacement. $E_n(\bar{\boldsymbol{r}}_{i0})$ is the envelope of the new displacement

$$E_n(\bar{\boldsymbol{r}}_{i0}) = 0.5 \times \left[\tanh\left(\theta\,||\bar{\boldsymbol{r}}_{i0} - \bar{\boldsymbol{e}}_z(\bar{\boldsymbol{e}}_z \cdot \bar{\boldsymbol{r}}_{i0})| - L_0|\right) - 1\right]. \quad (11)$$

Here $\bar{\boldsymbol{e}}_x, \bar{\boldsymbol{e}}_z$ are the unit vectors in the x and z axes, respectively. As shown in Fig. 2, the parameters denoted in Eq. (10) are as follows: Δq — the amplitude of the planar deflation, L_0 — the size of the intruded domain, θ — the domain boundary width and ΔX — the magnitude of the shear displacement. While $B_d(\bar{\boldsymbol{r}}_{i0})$ in Eq. (10) denotes the buckling pattern within the six membered ring, and it will be defined in detail in the text later. In Fig. 2 this buckling is symbolically denoted by a zigzag line.

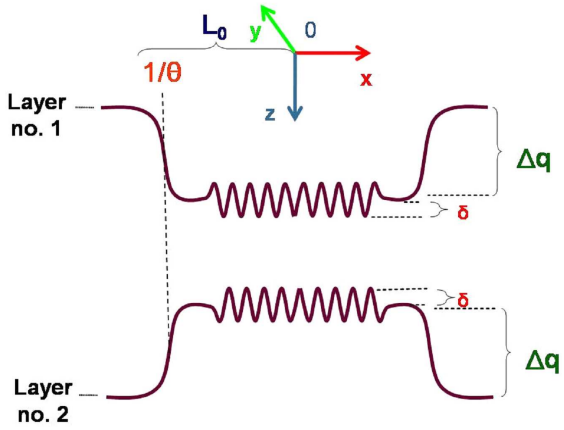

Fig. 2. The distortion pattern used in the calculations: Δq — the planar intrusion amplitude, δ — the buckling amplitude, L_0 — the system size, θ — the shape coefficient.

Inside of the intruded domain we thus introduce a buckling which is perpendicular to the layer with an amplitude δ. We will also assume that the center of mass of the six membered ring is preserved. The deformation of the second layer is assumed to be symmetric as shown in Fig. 2. Using this method, one can calculate the adiabatic energy of the domain formation for selected values of parameters. The key point is the top of the barrier or the stable point. The stable point formation is a result of competition of two processes: the σ-type inter-layer bond formation resulting in an energy gain, and the sp^2 type intra-layer bond tension resulting in an energy loss. As mentioned before, the energy required for the direct $sp^2 \rightarrow sp^3$ transition is rather high. Its main reason is a

long distance between neighboring layers (3.35 Å), while the inter-layer bond formation starts only at a short distance (≈ 2 Å [16]). Hence the displacement of the carbon atoms necessary to create intra-layer σ-type bonds takes considerable amounts of energy, if it occurs simultanously all over the crystal. However, in this case the distance is reduced within a locally intruded domain, so that the inter-layer bonds are created quite easily resulting in a lower energy barrier. The energetic cost of shortening the distance between the layers is spread over as a gradual tension at the border of the domain, and becomes much lower than in the case of a direct and global motion.

Using the pattern described in the previous section and the Brenner potential, we have performed the total cohesive energy calculations. By varying values of selected parameters $(\Delta q, \delta, \theta, L_0)$ we have obtained a potential energy surface (PES) of the conversion, with some extremal points indicating stable configurations of distorted structures. Our goal is to find such values of parameters $(\Delta q, \delta, \theta, L_0)$ which minimize the energy barrier between the initial graphite structure and a new one corresponding to a new stable point.

2.2. Results

Due to a large number of degrees of freedom of our system, there may be various possible buckling patterns. Hence we focus our attention on the following three ones.

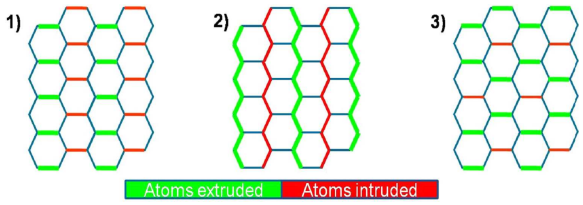

Fig. 3. The three patterns used in the calculations. (1) Pattern I — carbon atoms are intruded and extruded alternately along the z axis. (2) Pattern II — carbon atoms are intruded and extruded alternately (perpendicularly to pattern II along the z axis). (3) Pattern III applied in calculations with the additional shear displacement; two atoms forming regular line along the x axis direction are intruded with an amplitude δ, remaining atoms are extruded with the amplitude 0.5δ.

The first is the pattern I, where 3 carbon atoms within the six membered ring are equally extruded and intruded alternately along the z axis as shown in Figs. 3 and 4. The buckling function $B_d(\bar{\boldsymbol{r}}_{i0})$ in this case is thus determined.

The second one is the pattern II, where 3 carbon atoms within the six membered ring are equally extruded and intruded alternately along the z axis as shown in Figs. 3 and 5. The buckling function $B_d(\bar{\boldsymbol{r}}_{i0})$ in this case is thus determined.

The third one is the pattern III, where 4 of carbon atoms in the six membered ring are extruded and remaining 2 are intruded along the z axis, as shown in Figs. 3

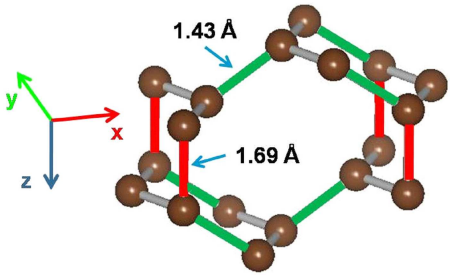

Fig. 4. The pattern I used in the calculations. Carbon atoms are intruded and extruded alternately along the z axis.

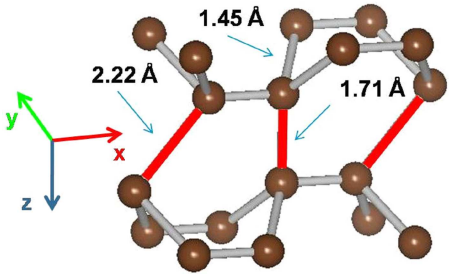

Fig. 5. Pattern II — carbon atoms are intruded and extruded alternately (pependicularly to pattern II) along the z axis.

and 6. In this case, in order to preserve center of mass, the amplitude of the buckling of extruded atoms is one half of intruded one. The buckling function $B_d(\bar{\boldsymbol{r}}_{i0})$ of this case is thus also determined. Furthermore, we apply additional shear displacement ΔX along the x axis as also shown in Fig. 6.

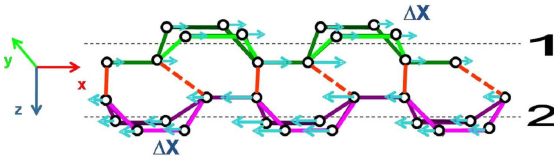

Fig. 6. The pattern III applied in calculations with the additional shear displacement; two atoms forming regular line along the x axis direction are intruded with an amplitude δ, remaining atoms are extruded with the amplitude 0.5δ. In order to optimize inter-layer the bond angles, both deflated domains are shifted relatively in the x direction, as denoted by ΔX (> 0).

Using the minimization technique described in the last section, we have performed large scale (80000 atoms) calculations using these three aforementioned patterns.

In the case of pattern I the total energy is shown in Fig. 7, wherein the horizontal axis denotes the total intrusion $(\delta + \Delta q)$, whose zero corresponds to the starting graphite. The energy barrier is $E_{\mathrm{b}} = 1.07$ eV, however the depth of the potential well representing a new phase is only 0.19 eV. At around $\delta + \Delta q \approx 0.7$ Å ~ 0.8 Å, we

have a maximum and a minimum, when $L_0 = 5.68$ Å, $\Delta q = 0.72$ Å, $\delta = 0.11$ Å, $\theta = 0.7$ (1/Å). The whole structure at this minimum is described in Fig. 4.

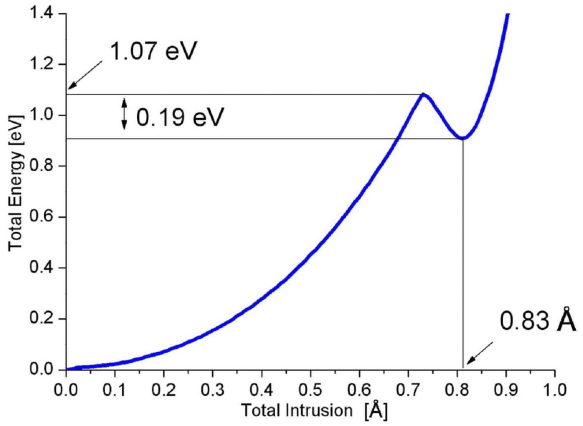

Fig. 7. The PES of the transformation with the pattern I. The horizontal axis indicates the total intrusion of the domain $(\delta + \Delta q)$. The second minimum occurs when the total intrusion becomes as $\delta + \Delta q = 0.83$ Å with an energy barrier 1.07 eV.

In the case of pattern II the total energy is shown in Fig. 8, wherein the horizontal axis denotes the total intrusion $(\delta + \Delta q)$, whose zero corresponds to the starting graphite. The energy barrier is $E_b = 1.29$ eV and the depth of the potential well representing a new phase is much larger but still rather shallow this time (0.28 eV). At around $\delta + \Delta q = 0.83$ Å, we have a minimum, when $L_0 = 5.68$ Å, $\Delta q = 0.67$ Å, $\delta = 0.15$ Å, $\theta = 0.8$ (1/Å). The whole structure at this minimum is described in Fig. 5.

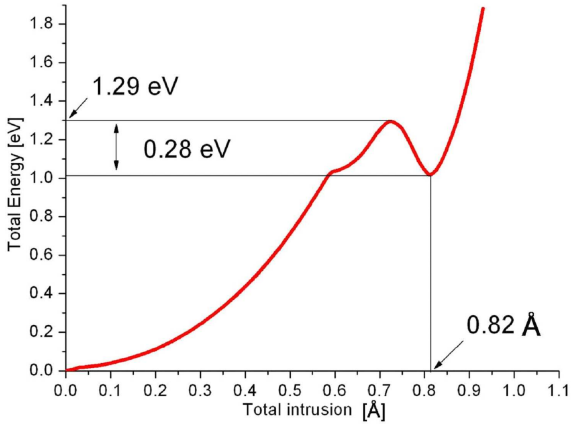

Fig. 8. The PES of the transformation with the pattern II. The horizontal axis indicates the total intrusion of the domain $(\delta + \Delta q)$. The second minimum occurs when the total intrusion becomes as $\delta + \Delta q = 0.82$ Å with an energy barrier 1.29 eV.

In the case of pattern III the calculated energy is shown in Fig. 9. Although the intrusion amplitude has the similar value to the case of the pattern I ($\Delta q = 0.67$ Å), in this case we obtain a nearly more than twice as large buckling amplitude, $\delta = 0.24$ Å. However, the energy barrier ($E_b = 0.88$ eV) becomes much lower than in the previous case. Furthermore, by shifting the layers in the opposite direction by $\Delta X = 0.35$ Å, we obtain a quite stable phase with the nearly 0.4 eV depth. In Fig. 10, we have shown the total energy in a 2D space, as a function of Δq and $(\delta + \Delta q)$. One finds that $\Delta q \approx 0.6$ Å and $\delta + \Delta q \approx 0.7$ Å ~ 0.8 Å corresponds to the barrier top, and for $\delta + \Delta q = 0.91$ Å, a stable domain is formed with σ-type inter-layer bonds. In Fig. 11, the whole structure at the new minimum is shown.

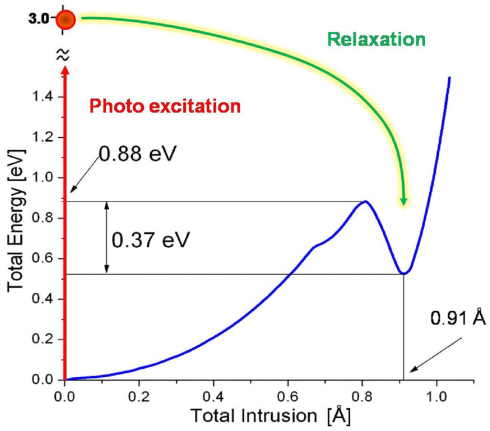

Fig. 9. The PES of the transformation with the pattern III. The horizontal axis indicates the total intrusion $(\delta + \Delta q)$ of the domain. The second minimum occurs when the total intrusion $\delta + \Delta q = 0.91$ Å with the energy barrier 0.88 eV. This energy barrier may be easily overcome by visible excitations (≈ 3 eV) and the system may reach the second minimum.

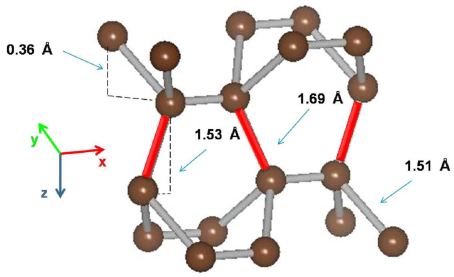

Fig. 11. The structure of the pattern III with the additional shear displacement.

Obviously, patterns I, II and III do not exhaust all the possible buckling patterns. So, we have examined various other buckling patterns. Though variety of (meta)stable phases would be observed with respective different depths of potential well, the lowest energy barrier occurs in patterns I and III.

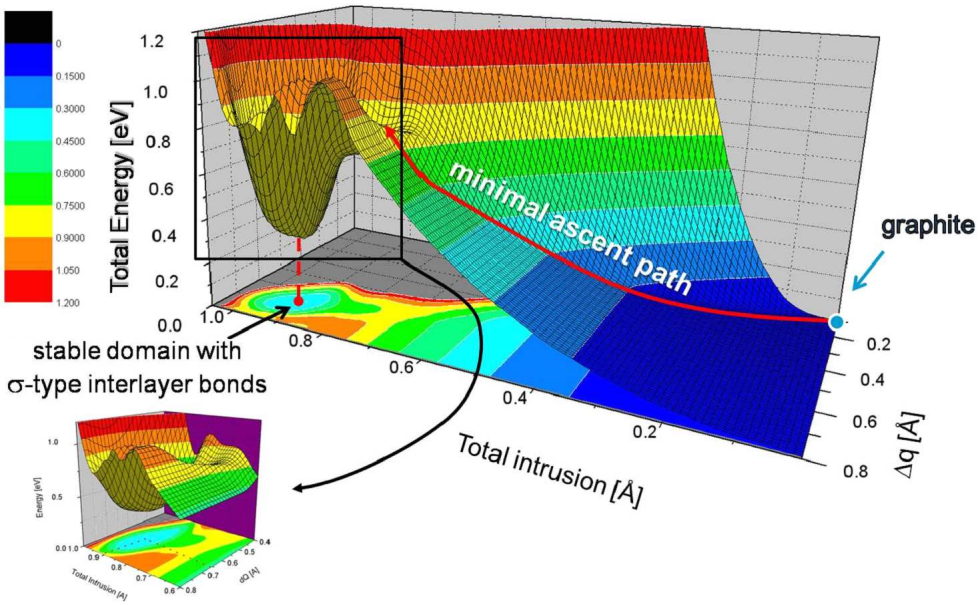

Fig. 10. The detailed PES of the structure with the pattern III. The total energy is plotted versus the total intrusion $(\delta + \Delta q)$ and intrusion amplitude Δq. When $\Delta q \approx 0.6$ Å and $\delta + \Delta q \approx 0.8$ Å a stable domain with σ-type inter-layer bonds is formed. The red line indicates the minimal ascent path from the starting graphite to the new domain structure.

One can conclude that the pattern III shown in Fig. 11 is the most possible domain. The energy barrier is of the order of 1 eV, being easily overcome by a few visible photons as schematically shown in Fig. 8. The resultant structure agrees well with the experiment [3, 4]. Moreover, if we take the average over the buckling within each layer, the new inter-layer distance is about 2 Å, which agrees well with the experiment [4, 5].

2.3. Size evolution

Though this paper is mostly concerned with phenomena which occur after initially overcoming the transition barrier, one may ask the question what is energetic size evolution of the system? The validity of the question is motivated by the possible scenario of the system growth.

As mentioned before, we may treat the energetic evolution of the system by the following, qualitative observation. The occurrence and height of the barrier is a result of the competition between energy loss due to intralayer's bond tension and energy gain due to intralayer bond formation. Henceforth we may induce that, from qualitative point of view, only the initial transition from graphite to "diaphite" should be expensive since we have to transform number of atoms proportional to L^2. Then further increasing size of the system would require to transform atoms only on the circumference of intruded domain. Hence the number of atoms on the circumference is now proportional only to L, we expect linear increase of energy barrier instead of exponential one, as in the case of direct transition.

The results of calculations using our method were presented in Fig. 12. The black line indicates height of energy barrier E_b of direct transition from graphite to "diaphite" with define value L. We may observe that with increasing value of L, E_b is getting higher rapidly from 0.88 eV up to 2.57 eV for $L = 12$ Å and 5.97 eV for $L = 24$ Å. From the other hand, the red line indicates evolution of energy barrier via indirect transition i.e. first overcoming the initial barrier and then increasing the size. The increase this time is much slower with 1.4 eV for $L = 12$ Å and 2.2 eV for $L = 24$ Å. The calcu-

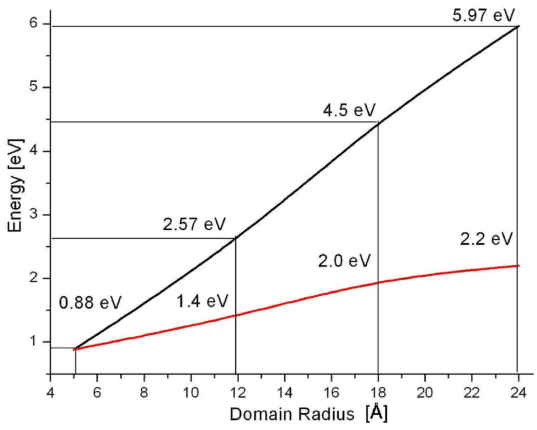

Fig. 12. Energy barrier of "diaphite" domain formation with respect to its radius. The black line indicates height of energy barrier E_b of direct transition from graphite to "diaphite" with defined value L. The red line indicates evolution of energy barrier via indirect transition i.e. first overcoming the initial barrier and then increasing the size.

lations conclude the hypothesis of system evolution and maybe connected with graphite–diamond conversion. In the case of heat and pressure transition much energy is required since transformation occurs simultaneously in large volume of the material. However with the help of photoexcitation it may be possible to conduct step by step conversion, as in the case of "diaphite" where only first step is of relatively full cost. However further increase of "diaphite" domain does not require large amounts of energy and it is possible to "jump" from one stable valley into another using small pulses.

Acknowledgments

This work was supported by State Committee of Scientific Research of Poland under grant no. 2290/B/H03/2009/37, year 2009.

References

[1] R. Saito, M. Fujita, G. Dresselhaus, M.S. Dresselhaus, *Phys. Rev. B* **46**, 1804 (1992).

[2] N. Chen, M.T. Lunes, A.C.T. van Duin, *Phys. Rev. B* **72**, 085416 (2005).

[3] L. Radosinski, K. Nasu, J. Kanazaki, K. Tanimura, A. Radosz, T. Luty, in: *Molecular Electronic and Related Materials — Control and Probe with Light, Naito Toshio, August 2009*, Trans-world Research Network Publisher, Kerala (India) 2010, p. 281.

[4] J. Kanasaki, E. Inami, K. Tanimura, H. Ohnishi, K. Nasu, *Phys. Rev. Lett.* **102**, 087402 (2009).

[5] R.K. Raman, Y. Murooka, C.-Y. Ruan, T. Yang, S. Berber, D. Tomanek, *Phys. Rev. Lett.* **101**, 077401 (2008).

[6] K. Nasu, *Photoinduced Phase Transitions*, World Sci., Singapore 2004.

[7] A. Radosz, K. Ostasiewicz, P. Magnuszewski, L. Radosinski, F.V. Kusmartsev, J.H. Samson, *Phys. Status Solidi B* **242**, 454 (2005).

[8] A. Radosz, K. Ostasiewicz, P. Magnuszewski, L. Radosinski, F.V. Kusmartsev, J.H. Samson, *Phys. Status Solidi B* **242**, 303 (2005).

[9] A. Radosz, K. Ostasiewicz, P. Magnuszewski, L. Radosinski, F.V. Kusmartsev, J.H. Samson, A.C. Mitus, G. Pawlik, *Phys. Rev. E* **73**, 026127 (2006).

[10] K. Nasu, *Rep. Prog. Phys.* **67**, 1607 (2004).

[11] S. Fahy, S.G. Louie, M.L. Cohen, *Phys. Rev. B* **35**, 7623 (1987).

[12] S. Fahy, S.G. Louie, M.L. Cohen, *Phys. Rev. B* **34**, 1191 (1986).

[13] F.P. Bundy, *Chem. Phys.* **38**, 631 (1963).

[14] T. Irifune, A. Kurio, S. Sakamoto, T. Inoue, H. Sumiya, *Nature* **421**, 599 (2003).

[15] H. Nakayama, H. Yoshida, *J. Phys. CM* **15**, R1077 (2003).

[16] D.W. Brenner, *Phys. Rev. B* **42**, 9458 (1990).